Key Points:

- Fluxes of galactic cosmic ray (GCR) protons were simulated using the daily modulation parameter, reconstructed from ground-based data
- The simulation results yield good agreement with the space-borne AMS-02 measurements for 2011–2019, especially for intermediate rigidities
- This verifies the validity of the daily modulation parameter and can be used to estimate GCR fluxes, for example, when AMS-02 data are unavailable

Correspondence to:

P. Väisänen,
pauli.vaisanen@oulu.fi

Simulation of Galactic Cosmic Ray Proton Fluxes With the Daily Modulation Parameter: Validation With AMS-02 Data for 2011–2019

Pauli Väisänen[1,2,3,4] 📷, **Bruna Bertucci**[3,4] 📷, **Nicola Tomassetti**[3,4], **Miguel Orcinha**[4] 📷, **Ilya Usoskin**[1,2] 📷, **and Sergey Koldobskiy**[1,2]

[1]Sodankylä Geophysical Observatory, University of Oulu, Oulu, Finland, [2]Space Physics and Astronomy Research Unit, University of Oulu, Oulu, Finland, [3]Department of Physics and Geology, University of Perugia, Perugia, Italy, [4]INFN Sezione di Perugia, Perugia, Italy

Abstract The flux of galactic cosmic rays (GCRs) is modulated by solar activity on different time scales. This is often described with the force-field approximation via the single variable parameters of the modulation parameter, which formally corresponds to the average rigidity loss of GCR particles in the heliosphere. The force-field approximation is usually assumed to work properly only for periods of a solar rotation (27 days) or longer. However, daily values of the modulation parameter have been constructed based on ground-based neutron monitor (NM) data suggesting that this approach might work reasonably well also on shorter time scales. Here we check this by simulating the daily GCR proton fluxes using the force-field approach and the daily modulation parameter reconstructions, and confronting them with the daily proton-flux measurements by the AMS-02 onboard the International Space Station. A polynomial regression between the simulated and measured fluxes is proposed for longer-term analyses and interpolations. For mid-rigidities from 5–15 GV, the agreement is accurate within ±1% and slightly worsens toward higher rigidities, likely because of smaller statistics. We also found a lingering solar-cycle trend at lower energies between the data and the model and the effect of the solar magnetic field polarity. These findings can be used for the utilization of the force-field approach for short-term variations.

1. Introduction

The flux of galactic cosmic rays (GCRs) entering the solar system encounters solar wind and the heliospheric magnetic field (HMF) and gets modulated by them (e.g., Potgieter, 2013). This leads to variations of the GCR flux with the pronounced 11-year solar dynamo cycle and the $\approx$ 27-day solar rotational period. In addition, short-term sporadic variability can be caused by interplanetary transients such as coronal mass ejections (CMEs) and interaction regions.

The effect of GCR modulation is often parameterized by the heliospheric modulation parameter ϕ, which is based on the force-field approximation (Gleeson & Axford, 1968) of the full cosmic-ray transport equation (Parker, 1965). A dimension-based interpretation of ϕ is that it describes the average rigidity loss of a particle inside the heliosphere, but because of the oversimplified nature of the force-field model, its exact physical meaning is obscure (Caballero-Lopez & Moraal, 2004). The modulation parameter is used as a formal parameter for simple modeling of the heliospheric modulation effects (Usoskin et al., 2005). Since the force-field model is based on the quasi-steady-state and spherically symmetric 1D approximation, it is typically assumed to be valid for assessing heliospheric modulation only roughly for monthly or longer timescales (Caballero-Lopez & Moraal, 2004; Usoskin et al., 2011). However, Väisänen et al. (2023) recently provided a reconstruction of the daily series of the modulation parameter based on careful examination of daily neutron monitor (NM) count rates and using a local interstellar spectrum (LIS) model from Vos and Potgieter (2015), and NM yield function from Mishev et al. (2020). An analysis of the result showed that the daily ϕ values also produce realistic results even during the periods of Forbush decreases caused by heliospheric transients (Usoskin et al., 2015). Ground level enhancement (GLE) events caused by solar energetic particles have a different nature and a different rigidity spectrum (Usoskin et al., 2020) and were excluded from the modulation parameter estimates.

In order to check the validity of the use of the modulation parameter on the daily timescale, we have simulated the daily GCR proton fluxes based on the force-field approximation with the daily ϕ values computed from NM data
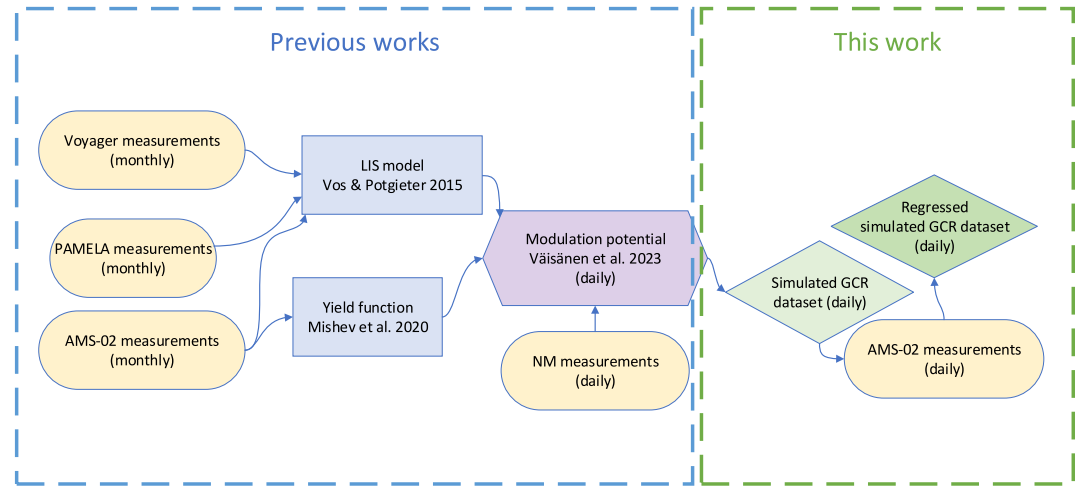
Figure 1. Flowchart of the process, used data and models used in this work.

and compared them with direct in-space measurements performed by the AMS-02 (Alpha Magnetic Spectrometer) instrument onboard the International Space Station (Aguilar et al., 2021a, 2021b). Since AMS-02 was also used as an input for the LIS and yield function models, the process essentially takes the higher sampling resolution data back to the space (or magnetosphere) environment. The overall process is depicted in Figure 1, which shows that the yield function (based on AMS-02 data) and the LIS model (based on Voyager, PAMELA and AMS-02 data) are used to create the daily modulation parameter using daily NM data, which then is used to create daily GCR fluxes and finally the regressed data with daily AMS-02 data.

Here, we focus on the ability of the force-field model and the modulation parameter to correctly describe the variability of the GCR proton fluxes as a function of rigidity on the daily timescale. If validated, this approach can be used for quick estimates of the variation of the GCR fluxes at different energies/rigidities based on NM data for interpolating and extrapolation direct data from AMS-02 and other direct GCR measurements.

In Section 2, we describe the data sets and the methodology used to simulate daily GCR proton fluxes. In Section 3 we present the simulated fluxes and compare them with the AMS-02 measurements, and in Section 4 we discuss the result, its parameter use as well as the forthcoming work.

2. Data and Methods

2.1. The Daily Modulation Parameter Estimate

This section describes how the daily modulation parameter used here was constructed by Väisänen et al. (2023) from the data of the worldwide NM network. Details can be found in that reference, but the procedure is briefly described here. The modulation parameter ϕ is the sole variable parameter in the force-field approximation of the Parker cosmic-ray transport equation. It assumes a steady-state and spherically symmetric heliosphere without internal cosmic ray sources and an initially negligible adiabatic energy loss rate. The modulated energy spectrum of protons near Earth can be then solved as

$$J_p(T, \phi) = J_{\text{LIS},p}(T + \Phi_p) \frac{(T)(T + 2T_p)}{(T + \Phi_p)(T + \Phi_p + 2T_p)}, \tag{1}$$

where $\Phi_p = e \cdot \phi$, ϕ being the modulation parameter, T the kinetic energy and T_p the proton's rest energy.

As the local interstellar spectrum (LIS) for particle species i we used the model provided by Vos and Potgieter (2015):

$$J_{\text{LIS}}(T) = C_i \cdot J_0 \cdot \frac{T^{1.12}}{\beta^2} \left(\frac{T + 0.67}{1.67} \right)^{-3.93}, \tag{2}$$
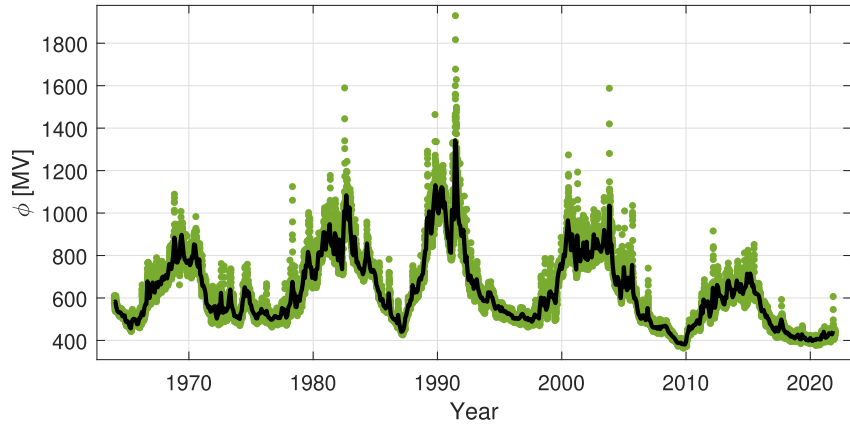
Figure 2. Monthly (black line) and daily (green dots) modulation parameter as reconstructed by Väisänen et al. (2023).

where C_i is the ratio of species i to protons (Koldobskiy et al., 2019; Väisänen et al., 2023), $J_0 = 2700$ (m^2 s sr GeV/nuc)$^{-1}$, and β is the ratio of the particle velocity to the speed of light. This LIS model is described in more detail in subsection 2.3.

Knowing the energy spectrum of cosmic rays, we can combine it with a neutron monitor yield function for the GCR species i, Y_i (Mishev et al., 2020), to estimate the theoretical count rate of a neutron monitor

$$N^*(\phi(t),\ R_c, h) = \sum_i \int_{T_{c,i}}^{\infty} Y_i(T, h)\ J_i(T, \phi(t))\ dT, \tag{3}$$

where $T_{c,i}$ is the kinetic energy of the species i corresponding to the geomagnetic rigidity cutoff R_c, h is the atmospheric depth, and summation is over the cosmic-ray species i, which is either proton or alpha particle for this yield function model. Heavier species are considered as scaled alpha-particles and effectively included in the C_i parameter in Equation 2. Although the integration is to infinity, for practical computation reasons we use the upper limit $T = 1,000$ GeV. The modulation parameter $\phi(t)$ was determined by Väisänen et al. (2023) by minimizing the merit function

$$M(t) = \sqrt{\frac{1}{X} \sum_{j=1}^{X} \left(1 - \frac{\kappa_j N_j(t)}{N_j^*(\phi(t), R_{c(j)}, h_j)}\right)^2}, \tag{4}$$

where X is the number of used NM stations, κ_j is the average scaling factor, accounting for the non-ideality of each NM station j, $N_j(t)$ is the measured NM count rate at the time t. The used 10 NM stations in (Väisänen et al., 2023) all had similar, low rigidity (<3 GV) cutoffs in order for better consistency of the used NM data and covering the full range of the rigidity spectrum. For future work, using more stations with wider range of cutoffs is planned.

The modulation parameter published in Väisänen et al. (2023) includes daily values from 1964 to 2021 and is shown in Figure 2. For this work, we focus on 2011–2019 since this period overlaps with published AMS-02 daily data, but also perform the computations and include results for the whole period in Section 3.

2.2. AMS-02 Daily Proton Data

AMS-02 is a state-of-the-art particle detector (Aguilar et al., 2021a, 2021b) which is set up onboard the International Space Station and aims to study cosmic-ray particles with energies up to 2 TeV. It started its operations in 2011 and is still operating.

The daily proton data for the period of 2011–2019 was published by Aguilar et al. (2021a, 2021b). While the measurements are continuing, real-time data is not available because of the complicated offline analysis. The measurements contain daily proton fluxes in 30 rigidity bins ranging from 1 to 100 GV as shown in Table 1. The

Table 1
The Rigidity Bins (in GV) in the AMS-02 Proton Data and Their Geometric Means

Bin start	Bin end	Geom. mean	Bin start	Bin end	Geom. mean	Bin start	Bin end	Geom. mean
1	1.16	1.077	3.29	3.64	3.461	8.48	9.26	8.861
1.16	1.33	1.242	3.64	4.02	3.825	9.26	10.1	9.671
1.33	1.51	1.417	4.02	4.43	4.220	10.1	11	10.540
1.51	1.71	1.607	4.43	4.88	4.650	11	13	11.958
1.71	1.92	1.812	4.88	5.37	5.119	13	16.6	14.690
1.92	2.15	2.032	5.37	5.9	5.629	16.6	22.8	19.455
2.15	2.40	2.272	5.9	6.47	6.178	22.8	33.5	27.637
2.40	2.67	2.531	6.47	7.09	6.773	33.5	48.5	40.308
2.67	2.97	2.816	7.09	7.76	7.417	48.5	69.7	58.142
2.97	3.29	3.126	7.76	8.48	8.112	69.7	100	83.487

table also shows the geometrical means $\sqrt{b_1 b_2}$ of the bins edges b_1 and b_2, which are used for selecting the bins for the synthetic data.

Rigidity R of a particle is often used instead of kinetic energy per nucleon T_i as it determines the trajectory of the particle in a magnetic field, regardless of the GCR particle species. The two quantities are related to each other as

$$R = \frac{A_i}{Z_i} \sqrt{T_i^2 + 2 \cdot T_i \cdot T_0}, \tag{5}$$

where A_i is the mass number, Z_i is the charge number and T_0 is the particle rest energy per nucleon (= T_p for protons). For protons, $A = Z = 1$.

An example of variations of the standardized (with the mean substracted and divided by the standard deviation) fluxes measured by AMS-02 in some rigidity channels are shown in Figure 3 along with the modulation parameter. This variation is a mix of the solar modulation effect and statistical fluctuations, with lower level of statistical fluctuations but stronger modulation seen for lower energies but higher level of statistical fluctuations and lower modulation for higher energies. The cosmic ray fluxes at different energies are anti-correlated with the modulation parameter. Modulation parameter values are continuous, whereas AMS-02 has some gaps, most notable at the end of 2014 and around 2018–2019.
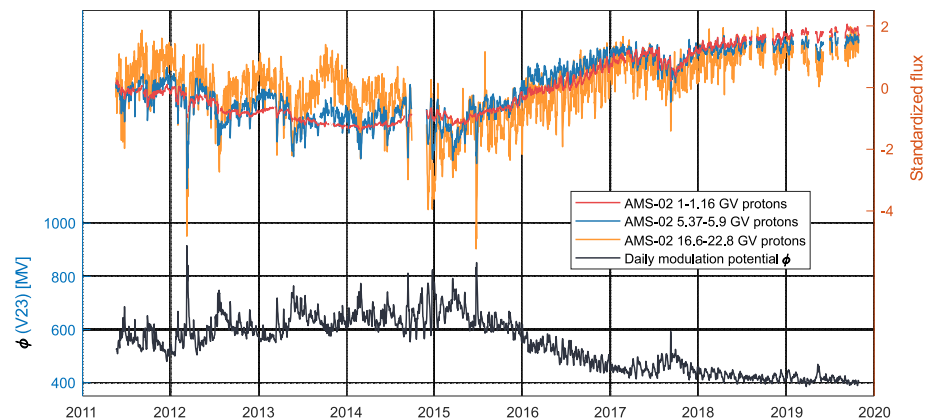

Figure 3. Upper panel, right-hand-side (RHS) *Y*-axis: Standardized daily proton fluxes measured by AMS-02 (Aguilar et al., 2021a, 2021b). Lower panel, LHS *Y*-axis: daily heliospheric modulation parameter values (Väisänen et al., 2023) for 2011–2019.
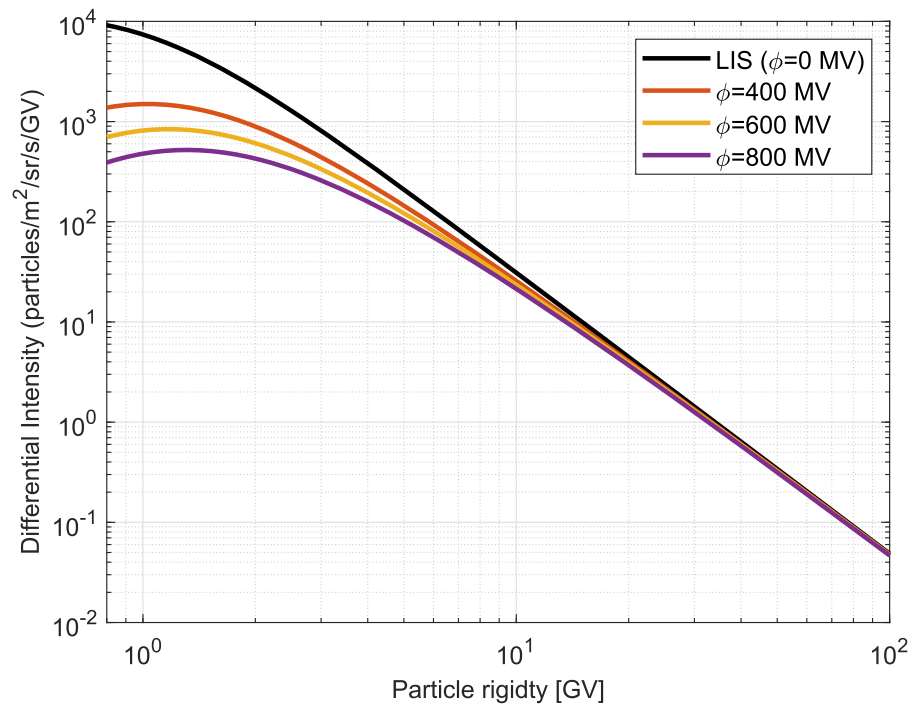
Figure 4. Modeled proton rigidity fluxes at different levels of modulation.

2.3. LIS Model

The force-field approximation includes the prescribed LIS (J_{LIS} in Equation 1) which determines the unmodulated particle energy spectrum outside the heliosphere. It is not a free parameter of the model but the values of ϕ slightly depend on the choice of LIS (Herbst et al., 2010; Usoskin et al., 2005). Thus, the LIS must be fixed for the force-field approach. For consistency, here we use the same LIS model (see Equation 2, Vos & Potgieter, 2015) as used by Väisänen et al. (2023) to compute the ϕ values.

The model LIS and different levels of modulation ranging from $\phi = 400–800$ MV are shown in Figure 4. The low level of modulation ($\phi \approx 400$ MV) corresponds to the solar cycle minimum after 2017, the medium level ($\phi \approx 600$ MV) corresponds to the average modulation during 2011–2016 and the high level ($\phi \approx 800$ MV) to high-activity episodes during 2012–2015, when the solar polarity reversal took place. Note that these levels refer to the period of 2011–2019 studied here, which was a weak solar cycle # 24. For other cycles, the maximum values of ϕ can reach 1600 MV (Figure 2).

3. Results

3.1. Proton Flux Time Series

Using Equations 1 and 2 and the daily values of the modulation parameter for 2011–2019, we simulated fluxes of protons in different rigidity bins according to Table 1. An example of the time evolutions of the standardized fluxes of protons with rigidities corresponding to the bins in Figure 3, is shown in Figure 5. In contrast to the AMS-02 data, where the variability of the standardized proton fluxes increases with energy/rigidity (Figure 3), the variability of the simulated fluxes (Figure 5) around the average are nearly identical for different rigidities. This is most likely related to the fact that the real AMS-02 data include statistical fluctuations whose relative contribution increases with rigidity, while the simulated data are "ideal" in the sense that their relative fluctuations are rigidity-independent, originating only from the
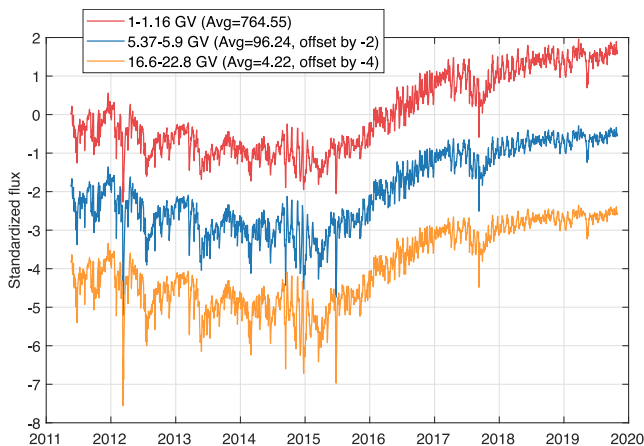

Figure 5. Simulated proton fluxes in three different rigidity bins as indicated in the legend. For clarity, the standard deviation lines are offset by −2 from one another.
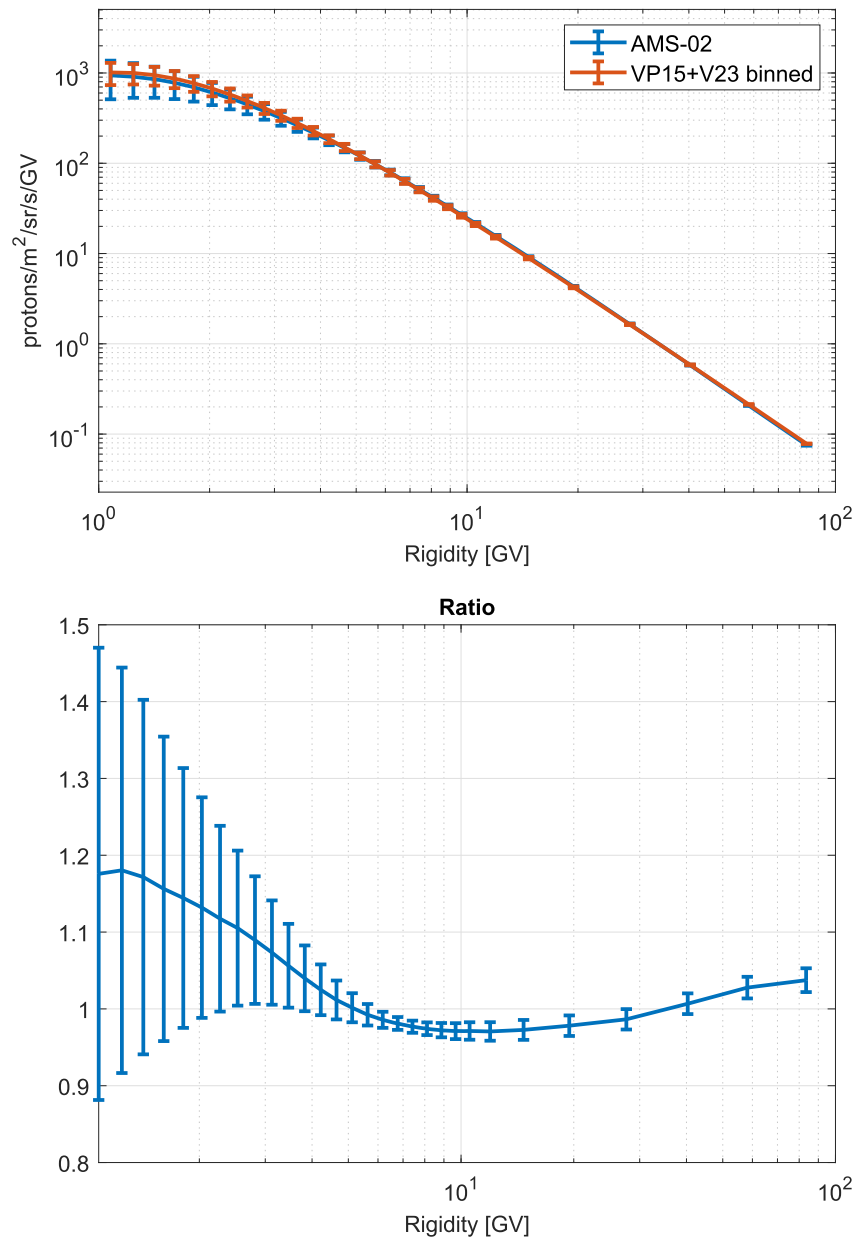
Figure 6. Upper panel: The average rigidity spectrum of protons for the period of 2011–2019 for the measured (blue) and simulated (red) fluxes, along with the standard deviation. Lower panel: Ratio of the simulated to the measured fluxes, shown in the upper plot, and its standard deviation.

fluctuations of the ϕ series. During strong Forbush decreases, observed as sharp dips, the different curves in Figure 5 have a noticeable difference between the rigidities because of the stronger modulated energy/rigidity spectrum.

Figure 6a shows the proton spectrum averaged over the entire studied period 2011–2019 along with its standard deviations for the simulated and measured by AMS-02 fluxes. The fluxes agree seemingly well, with only a slight difference in the lower rigidity part. To visualize the difference, in Figure 6b we show the ratio of the averaged fluxes shown in panel a and its standard deviation. The ratio exhibits a systematic pattern: while it is close to unity at higher rigidities, it is systematically higher at lower rigidities reaching the value of 1.18 at 1 GV. However, the ratio is roughly consistent with unity within the standard deviation under 5 GV rigidities. The ratio is within few
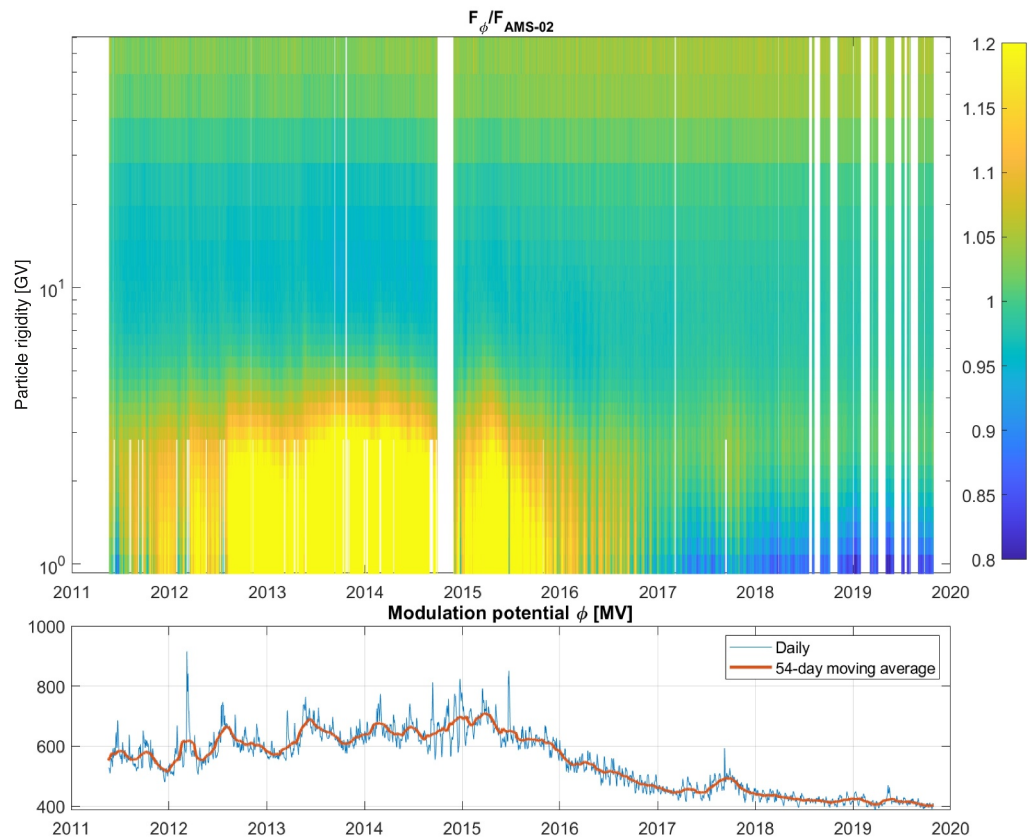
Figure 7. Top: The ratio of the modeled to measured spectra of daily GCR proton fluxes. Bottom: Daily modulation parameter and its 54-day moving average.

percent around unity in the rigidity range between 5–40 GV and starts slightly increasing toward higher rigidities reaching 1.04 ± 0.016 in the highest rigidity bin of 69.7–100 GV.

The temporal evolution of the ratio (see the lower panel of Figure 6) is shown in the upper panel of Figure 7. For the rigidity above ≈ 5 GV, the ratio is stable at about unity, implying the good agreement between the measured and simulated fluxes. For higher rigidities, the modulation of fluxes is low, and the ratio is anyway nearly constant around unity. For the lower rigidities below 5 GV, however, the ratio still varies significantly following the solar cycle, indicated by the modulation parameter in the lower panel. The model tends to slightly, within 20%, overestimate/underestimate the proton flux during the solar maximum/minimum conditions as compared to direct measurements, viz. slightly underestimating the modulation effect for low rigidities.

3.2. Scatter Analysis and Regression

In order to analyze the performance of the model at different rigidities, we made scatter plots of the measured and simulated proton fluxes for each rigidity bin individually, as shown in Figure 8. The color denotes the time evolution as indicated in the bottom panel. Red curves depict second-order polynomials fitted to the data, using the least-square method that can later be used to calibrate the simulated fluxes to the AMS-02 data. While the scatter is well confined around the diagonal for lower and mid-rigidity beans, especially between 5 and 15 GV, the spread is large at higher rigidities >20 GV where the statistical fluctuations of the measured values is greater than the expected modulation range, leading to the lost relationship. The model simulates flux variability which is indistinguishable in the measurements at the higher rigidities.

Interestingly, the shape of the best-fit second-order polynomial changes with rigidity. While for lower rigidities below 4 GV, the fit is concave, it becomes linear in the range from 4 to 7 GV and convex for higher rigidities. Moreover, the relationship between the modeled and measured fluxes is not homogeneous at different timescales: it is composed of multiple periods with nearly linear fits. This is illustrated in Figure 9 showing the scatter plot for
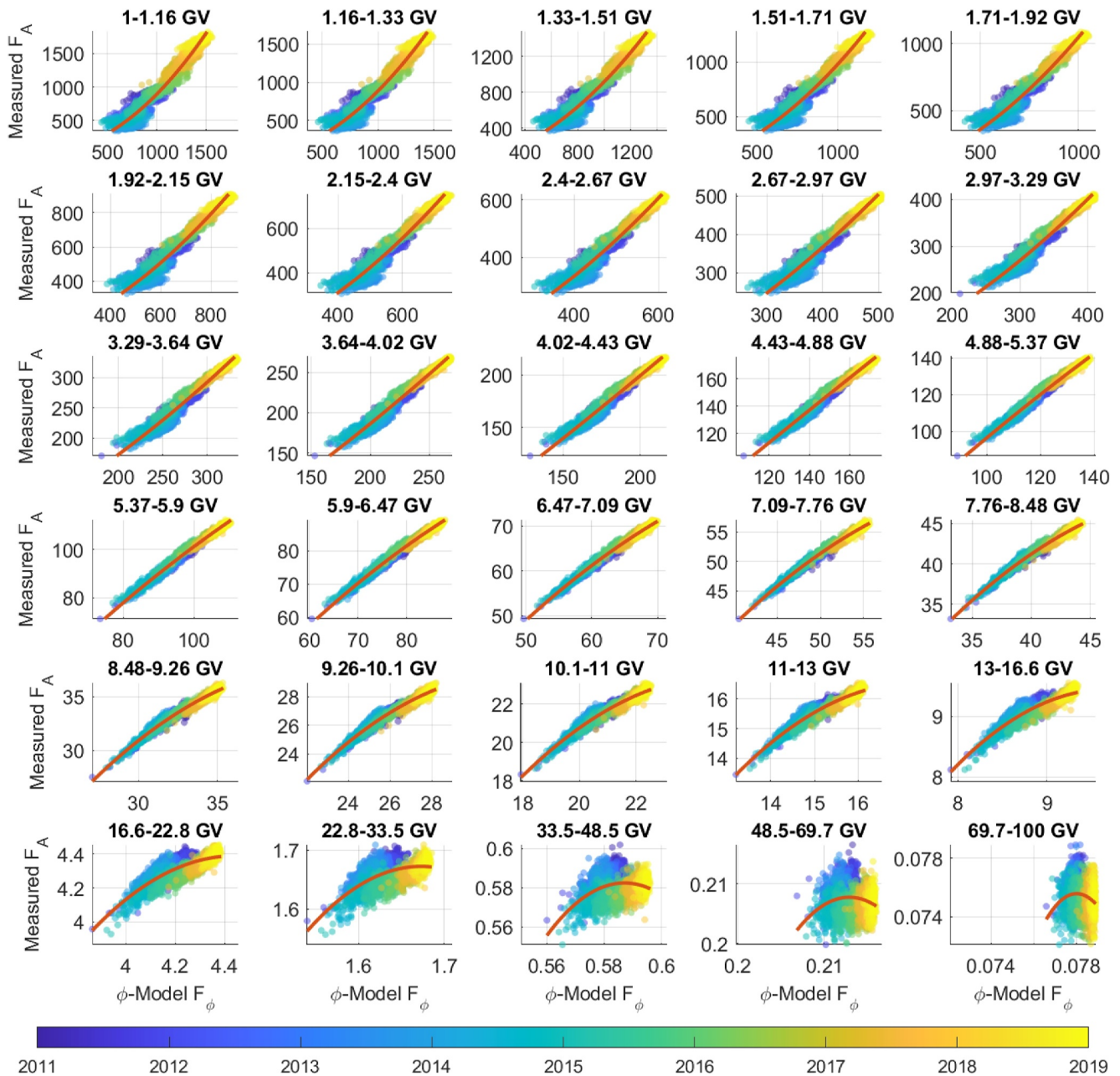
Figure 8. Scatter plots of the daily proton fluxes (in units of protons/m^2/sr/s/GV) for the simulations and measurements with the color indicating the date (see the color scale in the bottom). The red curves depict the best-fit second-order polynomials.

the bin of 1–1.16 GV (the first panel in Figure 8). As seen, the relationship is flatter and nearly linear at shorter timescales, as depicted by the dashed lines, that move along the diagonal. This indicates that, while the force-field model reproduces the average long-term modulation, it may be less precise at short timescales for lower rigidities especially during strong modulation.

For higher rigidities, the relationship exhibits a hysteresis-type behavior, related to the solar polarity reversal, which finished in November 2014 (Janardhan et al., 2018) but for both poles stabilized at around 2015. An example for the 16.6–22.8 GV bin is shown in Figure 10, where two branches can be seen: the one before 2014 (blue-colored) and another after 2016 (yellow-colored). This result is very similar to analysis performed in Mangeard et al. (2018), where results from low and high rigidity cut-off stations were compared. They also observed a type of plateau between the compared stations' count rates for the 2010–2014 period, and linear for
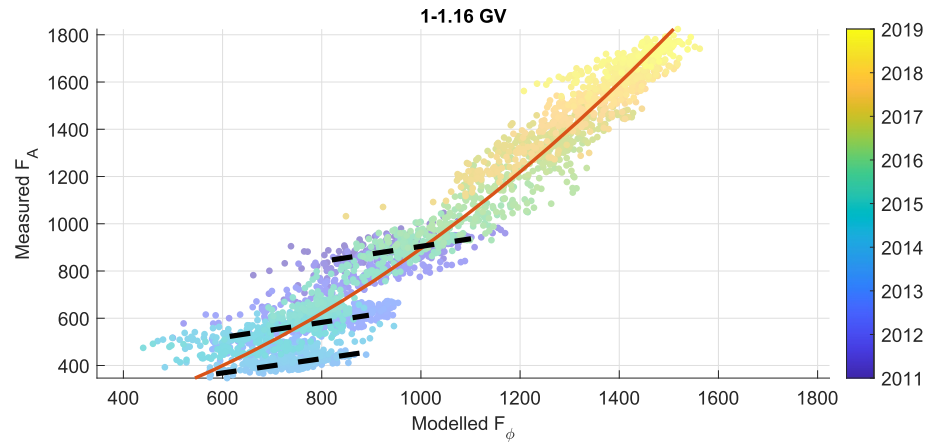
Figure 9. Scatter plot of the measured versus simulated fluxes of protons in the 1–1.16 GV rigidity bin. Notations are similar to Figure 8. Nearly linear short-term relationships are indicated by dashed lines.

2007–2010 and 2014–2017. Based on their results, this hysteresis effect seems to be related to the solar maximum and polarity reversal process than the polarity mode, which might seem to be the case without knowledge of data prior to 2010. Ultimately, it is the increased heliospheric current sheet tilt angle, which causes modulation at low rigidities that does not adhere to the force-field model, resulting in the uneven ratios between observed and modeled fluxes at high rigidities. Comparable results on can also be seen from leader fraction analysis in Banglieng et al. (2020), where the modulation effects for the 2010–2014 period are different. Accordingly, performing the fit separately for solar polarity reversal periods can potentially improve the parameterization. For the current work, we did not go into details of each individual rigidity bin to optimize the best fit, which is left for forthcoming work.

For the highest rigidities above 33.5 GV, the relation between the modeled and measured fluxes breaks. This is partly due to the hysteresis effects but mainly due to the fact that the modulation effect is very small at high rigidities and is hindered by the measurement fluctuations caused by low statistics of the higher rigidity particles.

The parameters of the second-order polynomial fit are tabulated in Table 2. They can be used to improve the ϕ-based GCR flux estimate F_ϕ and better match the modulated (AMS-02) GCR flux in units of protons/m^2/sr/s/GV for the rigidity bins j via the equation

$$F_j = a_j \cdot F_{\phi j}^2 + b_j \cdot F_{\phi j} + c_j. \tag{6}$$
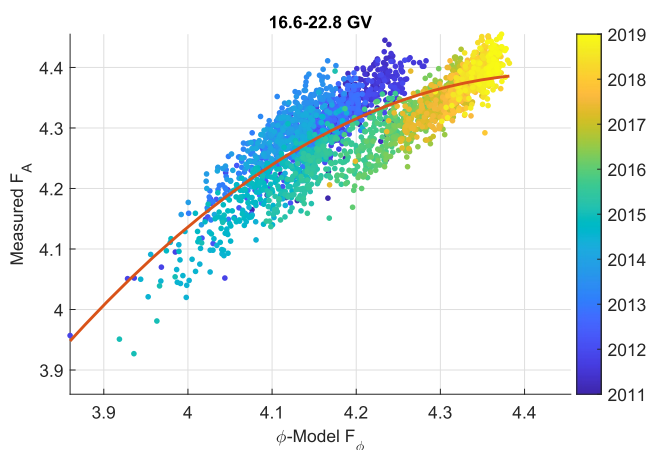
The regression can be used to calibrate the model results to AMS-02 measurements, which can be useful for, for example, interpolation or extrapolation of the fluxes beyond the periods when direct space-borne data is directly available. In Figure 11, we showcase the AMS-02 measurements, the model results and the 2nd-order regressed model results and their individual ratios for the rigidity bins $1 - 1.16$ GV, $5.37 - 5.9$ GV and $16.6 - 22.8$ GV, that were used as examples before. There is a systematic excess of the modeled flux over the measured one in the lowest energy bin (Figure 11 upper panels), especially around the solar maximum in 2013–2014, and lower values after 2016. By applying the regression discussed above, we can match the flux levels after 2016, but the values during the maximum years are still not fully corrected. For further calibration, another LIS model with smaller low-rigidity fluxes, or a more extensive ad-hoc calibration, can be used. Interestingly, the agreement between the model and the data is good for the year 2015, during the declining solar cycle phase, which was also characterized by high modulation. For medium rigidity (middle panels in Figure 11), the agreement is good, within a few per cent. By applying the correcting

Figure 10. Zoom in to the 16.6–22.8 GV bin of Figure 8.

Table 2
Parameters of the Second-Order Polynomial Fit for the Different Rigidity Bins (See Equation 6) in Units of (Protons/m²/sr/s/GV)

Bin [GV]	$a\,[F_\phi^2]$	$b\,[F_\phi]$	c
1.00–1.16	6.4269E−04	2.1067E−01	4.1459E+01
1.16–1.33	6.1585E−04	2.4175E−01	3.2242E+01
1.33–1.51	6.1980E−04	2.7415E−01	2.5943E+01
1.51–1.71	6.5902E−04	2.8884E−01	2.8314E+01
1.71–1.92	6.9034E−04	3.3783E−01	1.9304E+01
1.92–2.15	7.5043E−04	3.6934E−01	1.7001E+01
2.15–2.40	8.3337E−04	3.9775E−01	1.6317E+01
2.40–2.67	8.7567E−04	4.7798E−01	4.1408E+00
2.67–2.97	8.9866E−04	5.7577E−01	−7.1826E+00
2.97–3.29	1.1883E−03	4.8293E−01	1.7743E+01
3.29–3.64	1.1276E−03	6.3676E−01	2.7083E−01
3.64–4.02	8.9716E−04	8.2799E−01	−1.5076E+01
4.02–4.43	4.8496E−04	1.0270E+00	−2.5479E+01
4.43–4.88	−2.1401E−04	1.2439E+00	−3.3019E+01
4.88–5.37	−1.6575E−03	1.5474E+00	−4.1779E+01
5.37–5.90	−3.8252E−03	1.8578E+00	−4.6205E+01
5.90–6.47	−7.3590E−03	2.2283E+00	−4.9677E+01
6.47–7.09	−1.1705E−02	2.5130E+00	−4.7450E+01
7.09–7.76	−1.9756E−02	2.9946E+00	−4.8980E+01
7.76–8.48	−3.0574E−02	3.4402E+00	−4.7467E+01
8.48–9.26	−4.6714E−02	3.9632E+00	−4.5924E+01
9.26–10.1	−7.0759E−02	4.5784E+00	−4.4324E+01
10.1–11.0	−1.0041E−01	5.0614E+00	−4.0317E+01
11.0–13.0	−1.7754E−01	6.1789E+00	−3.7196E+01
13.0–16.6	−4.2810E−01	8.3096E+00	−3.0874E+01
16.6–22.8	−1.3259E+00	1.1779E+01	−2.1769E+01
22.8–33.5	−6.2079E+00	2.0769E+01	−1.5699E+01
5–48.5	−3.6655E+01	4.3037E+01	−1.2050E+01
5–69.7	−1.5274E+02	6.5022E+01	−6.7124E+00
7–100	−8.6750E+02	1.3534E+02	−5.2032E+00

regression, we can reduce the difference and achieve a very good match between the two. This rigidity range corresponds to the range that the used low-rigidity cutoff NM's are most sensitive to (Asvestari et al., 2017; Gieseler et al., 2017). The red curve could quite safely be used to fill in AMS-02 data gaps at the end of 2014 and in 2018–2019. For higher rigidity (lower panels), both the straightforward and regression-corrected models perform generally well.

Overall, the period around 2015–2016 shows up as a shift in the ratio. It follows the solar magnetic field polarity reversal, and it seems that during the $A > 0$ polarity, the model is in a better agreement with the measurements.

The studied ratios between the simulated and measured proton fluxes in all rigidity bins are shown in Figure 12, which includes the ratios, their standard deviations, maximum and minimum daily values, and the squared Pearson's correlation coefficient R^2 for the second-order polynomial fit. As seen, the regression corrected model provides a better fit yielding the ratios close to unity.

3.3. Proton Fluxes 1964–2021

The simulated GCR flux based on straightforward or empirically corrected force-field modeling can be used to fill the gaps in AMS-02 data but also extend it as pseudo-AMS data for the entire period of the modulation parameter available from 1964 onward. Figure 13 shows the time profiles of the proton fluxes in three rigidity bins modeled for 1964–2021. It is seen that the recent cycle 24, covered by the AMS-02 data, was quite small compared to the previous four cycles. Thus, the modeled proton fluxes involve extrapolation not only in time but also in the range of modulation.

In the forthcoming work, we plan to work on the cross-analysis of multiple data sets and improved fits to the AMS-02 data. However, this simulated daily data set can already be useful for interpolation and analysis purposes, as its deviations from the measured data are small, within 20% for lower rigidities and within 2% for higher rigidities.

4. Conclusion

Based on the modulation parameter computed from the worldwide NM network data (Väisänen et al., 2023) and the force-field approximation, we simulated the daily fluxes of GCR protons at specific rigidities and compared them to those directly measured by AMS-02 in space, for the period 2011–2019. The overall agreement is good, with the average modeled fluxes compared to measured ones being within 20% for low rigidities <4 GV and within 2% for higher rigidities. However, the difference is systematic. For lower rigidities from 1 to 5 GV, the simulated fluxes are on average up to 18% higher than the measured ones. Moreover, the ratio of the daily fluxes exhibits a solar-cycle variation. This small systematic difference can be related to an inadequacy of the used LIS model or to the fact that the modulation parameter is computed from NMs count rates which include not only protons but also heavier species but applied here to protons only.

For rigidities from around 5 GV to around 20 GV, the agreement is nearly perfect with the simulated fluxes matching the measured ones with ±1% standard deviation, while the maximum/minimum differences of individual daily data points are within ±5%. This rigidity range roughly corresponds to the effective energy range of low cutoff-rigidity NMs (Asvestari et al., 2017; Gieseler et al., 2017), which were used for determining the ϕ parameter. For higher rigidities above 20 GV, the agreement becomes rougher, probably due to inadequacy of the
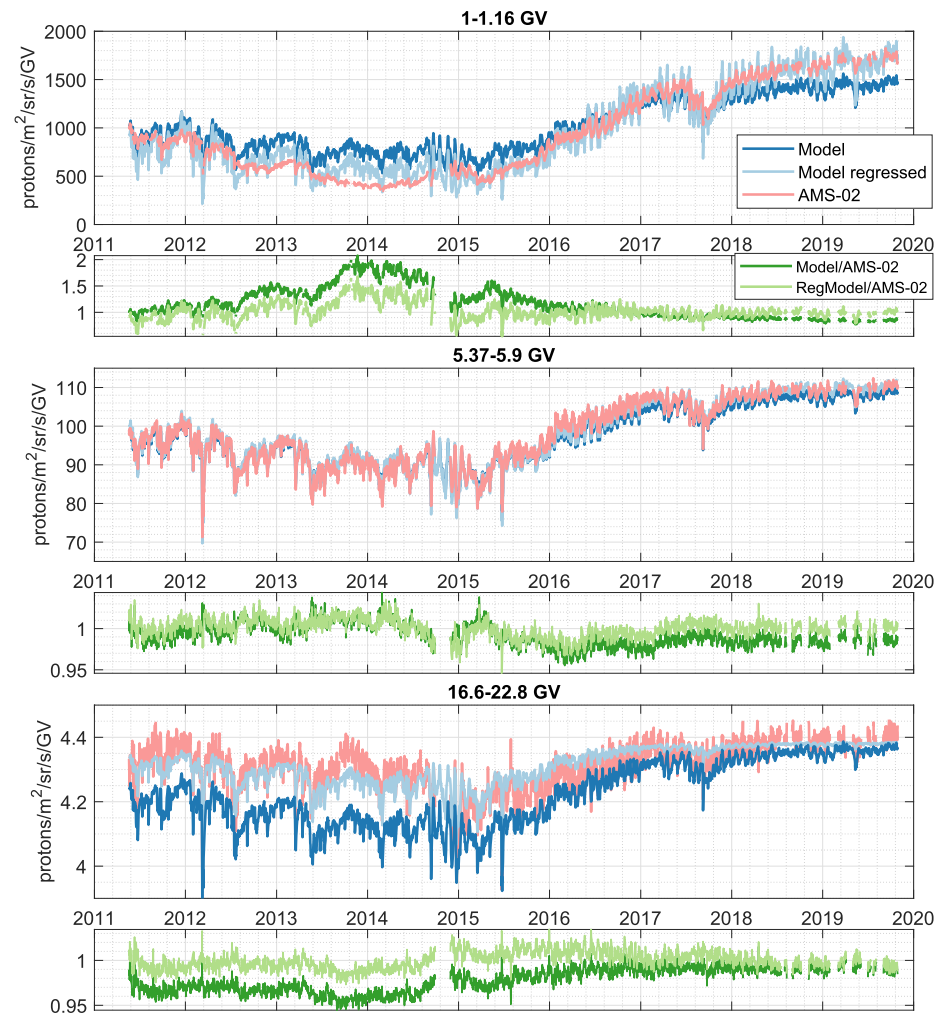
Figure 11. Proton fluxes as measured by AMS-02 (red) and the modeled ones, with (light blue) and without (blue) regression corrections, for three different rigidity bins along with the ratios of the modeled fluxes to the measured ones (light green with corrections and green without).

force-field approximation to assess modulation during solar polarity reversal and the resulting high heliospheric current sheet tilt (Mangeard et al., 2018). Another reason of increased statistical fluctuations in the data can be caused by reduced level of overall modulation so that the fluctuations becomes compatible with the modulation range.

Using the same approach, we also simulated the proton fluxes for the period of 1964–2021 period. This can be used to fill the gaps in the AMS-02 data set or extend it beyond the period of the available measurements. Similar methodology can also be applied to even longer period using the ϕ reconstructions, such as those by Usoskin et al. (2017) since 1951, Usoskin et al. (2005) since 1936, and Owens et al. (2024) since 1845, or even Usoskin et al. (2021) since 950, with monthly or annual resolutions.

Here, we provide a basic method to model the flux of GCR protons in a broad range of rigidities, which still has small but systematic discrepancies with the data, and more work on the topic is still needed to improve the relationship. Here we investigated only GCR protons, but helium and heavier ions also need to be analyzed as they form a significant fraction of the GCR flux. Measurements from other particle detectors also need to be considered, for example, from PAMELA (Picozza et al., 2013) and other long-term space instruments measuring GCR. The LIS model used here (Vos & Potgieter, 2015) gives good results, but there are other models (e.g., Boschini et al., 2020) that can be used, especially to address the discrepancy at lower energies. Also, the

Energy bin	Model/AMS-02					Regressed model/AMS-02			
	Average ratio	Std	Max. Ratio	Min. Ratio	R^2	Average ratio	Std	Max. Ratio	Min. Ratio
1-1.16 GV	1.1758	0.2943	2.0756	0.7731	0.9431	1.0221	0.1617	1.6769	0.5446
1.16-1.33 GV	1.1804	0.2638	1.9597	0.8147	0.9433	1.0177	0.1436	1.5953	0.5736
1.33-1.51 GV	1.1716	0.2307	1.8301	0.8515	0.9436	1.0139	0.1261	1.5119	0.6008
1.51-1.71 GV	1.1563	0.1981	1.7208	0.8801	0.9452	1.0105	0.1088	1.4347	0.6358
1.71-1.92 GV	1.1444	0.1691	1.6264	0.9103	0.9458	1.0080	0.0940	1.3851	0.6713
1.92-2.15 GV	1.1319	0.1435	1.5477	0.9338	0.9474	1.0060	0.0804	1.3206	0.7053
2.15-2.4 GV	1.1174	0.1209	1.4588	0.9493	0.9496	1.0044	0.0685	1.2558	0.7339
2.4-2.67 GV	1.1052	0.1009	1.3863	0.9669	0.9517	1.0032	0.0581	1.2133	0.7676
2.67-2.97 GV	1.0896	0.0830	1.3113	0.9794	0.9541	1.0023	0.0490	1.1746	0.7923
2.97-3.29 GV	1.0733	0.0679	1.2581	0.9800	0.9561	1.0017	0.0417	1.1458	0.8386
3.29-3.64 GV	1.0562	0.0545	1.2010	0.9772	0.9603	1.0011	0.0344	1.1102	0.8488
3.64-4.02 GV	1.0398	0.0428	1.1528	0.9718	0.9649	1.0008	0.0281	1.0819	0.8762
4.02-4.43 GV	1.0249	0.0330	1.1138	0.9662	0.9698	1.0005	0.0226	1.0670	0.8898
4.43-4.88 GV	1.0116	0.0253	1.0864	0.9606	0.9746	1.0003	0.0180	1.0560	0.9162
4.88-5.37 GV	1.0015	0.0189	1.0657	0.9610	0.9789	1.0002	0.0143	1.0450	0.9255
5.37-5.9 GV	0.9924	0.0140	1.0438	0.9552	0.9825	1.0001	0.0113	1.0349	0.9458
5.9-6.47 GV	0.9858	0.0105	1.0377	0.9513	0.9848	1.0001	0.0092	1.0345	0.9596
6.47-7.09 GV	0.9811	0.0083	1.0163	0.9531	0.9858	1.0001	0.0078	1.0347	0.9737
7.09-7.76 GV	0.9768	0.0079	1.0110	0.9482	0.9839	1.0001	0.0073	1.0379	0.9737
7.76-8.48 GV	0.9742	0.0083	1.0088	0.9440	0.9804	1.0001	0.0071	1.0304	0.9729
8.48-9.26 GV	0.9723	0.0093	1.0091	0.9403	0.9720	1.0001	0.0076	1.0398	0.9721
9.26-10.1 GV	0.9711	0.0104	1.0062	0.9390	0.9606	1.0001	0.0079	1.0356	0.9730
10.1-11 GV	0.9713	0.0114	1.0150	0.9346	0.9418	1.0001	0.0086	1.0323	0.9681
11-13 GV	0.9706	0.0121	1.0112	0.9358	0.9190	1.0001	0.0086	1.0320	0.9721
13-16.6 GV	0.9727	0.0130	1.0186	0.9370	0.8463	1.0001	0.0092	1.0293	0.9715
16.6-22.8 GV	0.9781	0.0134	1.0154	0.9446	0.6828	1.0001	0.0096	1.0344	0.9731
22.8-33.5 GV	0.9864	0.0133	1.0252	0.9477	0.3975	1.0001	0.0095	1.0328	0.9683
33.5-48.5 GV	1.0067	0.0135	1.0538	0.9657	0.1306	1.0001	0.0096	1.0319	0.9677
48.5-69.7 GV	1.0277	0.0141	1.0658	0.9845	0.0396	1.0001	0.0108	1.0388	0.9592
69.7-100 GV	1.0374	0.0155	1.0902	0.9862	0.0441	1.0002	0.0129	1.0435	0.9576

Figure 12. Statistics of the ratios between AMS-02 versus model and regressed model. Color coding is white for values of 1 (unity), orange for ±25% difference or over from unity except for the standard deviations, which are white and orange at 0 and 0.25, respectively. For R^2 the shading is white at unity and orange at 0.75 and lower. The shading changes linearly between the values.

knowledge of the NM yield function (Mishev et al., 2020) is important for modulation parameter methodology, and its possible inconsistency can be translated into the uncertain modulation parameter reconstruction. The force-field model also leaves out many physical effects, such as the charge-sign dependency (Nuntiyakul et al., 2014), which means that either the force-field model needs to be modified or these effects needs to be estimated with separate methods.

The modulation parameter, which is the sole variable parameter in the force-field approximation, is very useful for estimating the modulation of galactic cosmic rays and the related solar activity and limitations of the force-field model. Specifically, here we show that the modulation parameter can be feasible to utilize also at daily resolution. Future work in developing and testing longer, even higher sampling rate estimations of ϕ can be interesting and useful for improving the understanding of both long- and short-term solar variability and the changes in the radiation environment it causes.
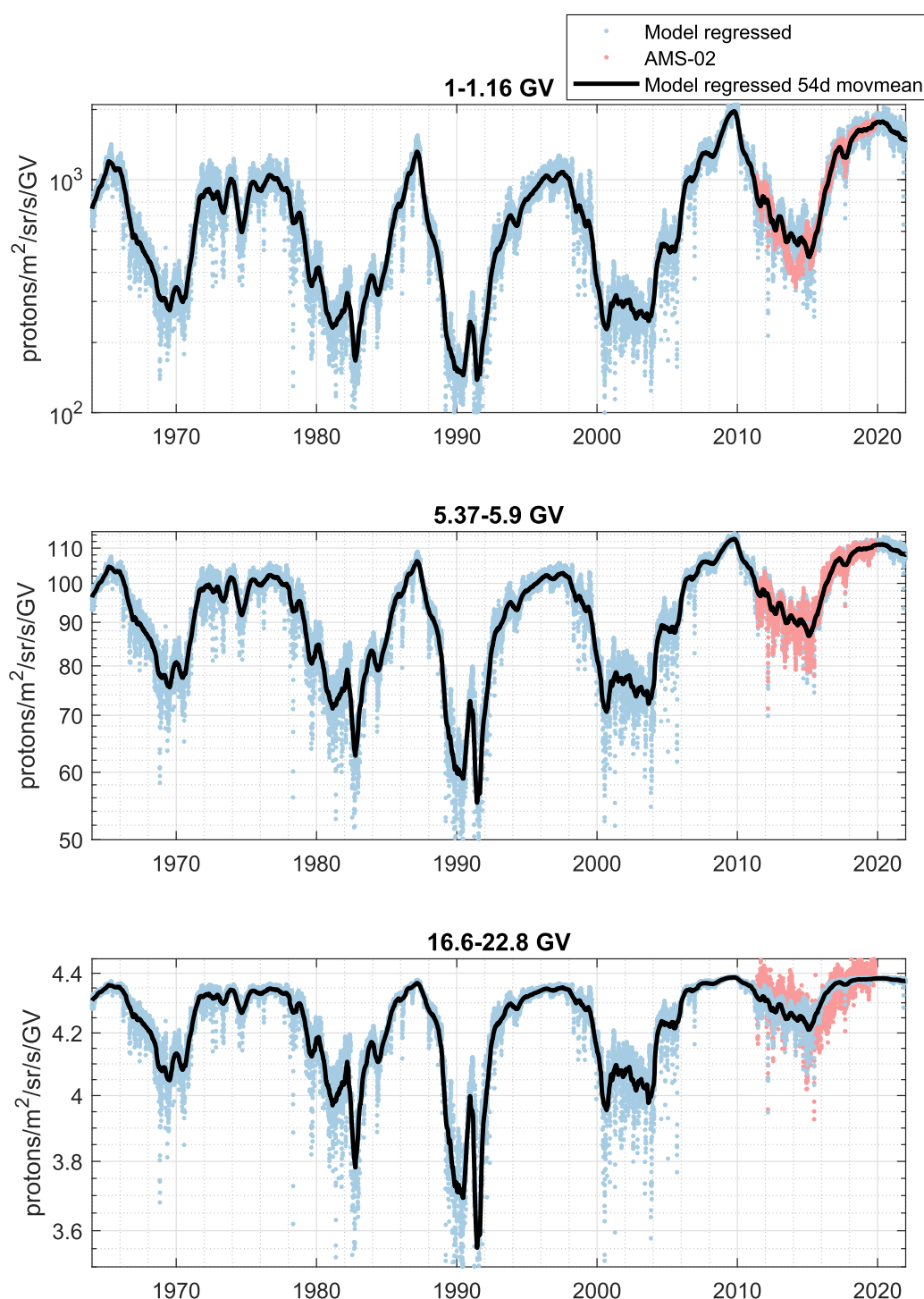
Figure 13. Time evolution of the daily proton fluxes for the period of 1964–2021 for three rigidity bins. Shown are the regression-corrected (light blue), its 182-day moving average and directly measured by AMS-02 (light red) data.

Data Availability Statement

The model and regressed model results for the rigidity bins (see Table 1) for both 2011–2019 and 1964–2021 are published in Fairdata.fi -repository (citation: Väisänen (2024, Dataset, CC4 BY-NC)).

References

Aguilar, M., Ali Cavasonza, L., Ambrosi, G., Arruda, L., Attig, N., Barao, F., et al. (2021a). The Alpha Magnetic Spectrometer (AMS) on the international space station: Part II — Results from the first seven years. *Physics Reports*, *894*, 1–116. https://doi.org/10.1016/j.physrep.2020.09.003

Aguilar, M., Cavasonza, L. A., Ambrosi, G., Arruda, L., Attig, N., Barao, F., et al. (2021b). Periodicities in the daily proton fluxes from 2011 to 2019 measured by the alpha magnetic spectrometer on the International Space Station from 1 to 100 GV. *Physical Review Letters*, *127*(27), 271102. https://doi.org/10.1103/PhysRevLett.127.271102

Asvestari, E., Gil, A., Kovaltsov, G. A., & Usoskin, I. G. (2017). Neutron monitors and cosmogenic isotopes as cosmic ray energy-integration detectors: Effective yield functions, effective energy, and its dependence on the local interstellar spectrum. *Journal of Geophysical Research: Space Physics*, *122*(10), 9790–9802. https://doi.org/10.1002/2017JA024469

Banglieng, C., Janthaloet, H., Ruffolo, D., Sáiz, A., Mitthumsiri, W., Muangha, P., et al. (2020). Tracking cosmic-ray spectral variation during 2007–2018 using neutron monitor time-delay measurements. *The Astrophysical Journal*, *890*(1), 21. https://doi.org/10.3847/1538-4357/ab6661

Boschini, M. J., Torre, S. D., Gervasi, M., Grandi, D., Jóhannesson, G., Vacca, G. L., et al. (2020). Inference of the local interstellar spectra of cosmic-ray Nuclei Z ≤ 28 with the GalProp-HelMod framework. *The Astrophysical Journal - Supplement Series*, *250*(2), 27. https://doi.org/10.3847/1538-4365/aba901

Caballero-Lopez, R. A., & Moraal, H. (2004). Limitations of the force field equation to describe cosmic ray modulation. *Journal of Geophysical Research: Space Physics*, *109*(A1). https://doi.org/10.1029/2003JA010098

Gieseler, J., Heber, B., & Herbst, K. (2017). An empirical modification of the force field approach to describe the modulation of galactic cosmic rays close to Earth in a broad range of rigidities. *Journal of Geophysical Research: Space Physics*, *122*(11), 10964–10979. https://doi.org/10.1002/2017JA024763

Gleeson, L. J., & Axford, W. I. (1968). Solar modulation of galactic cosmic rays. *The Astrophysical Journal*, *154*, 1011. https://doi.org/10.1086/149822

Herbst, K., Kopp, A., Heber, B., Steinhilber, F., Fichtner, H., Scherer, K., & Matthiä, D. (2010). On the importance of the local interstellar spectrum for the solar modulation parameter. *Journal of Geophysical Research*, *115*(D1), D00I20. https://doi.org/10.1029/2009JD012557

Janardhan, P., Fujiki, K., Ingale, M., Bisoi, S. K., & Rout, D. (2018). Solar cycle 24: An unusual polar field reversal. *A&A*, *618*, A148. https://doi.org/10.1051/0004-6361/201832981

Koldobskiy, S. A., Bindi, V., Corti, C., Kovaltsov, G., & Usoskin, I. (2019). Validation of the neutron monitor yield function using data from AMS-02 experiment 2011 – 2017. *Journal of Geophysical Research: Space Physics*, *124*(4), 2367–2379. https://doi.org/10.1029/2018JA026340

Mangeard, P.-S., Clem, J., Evenson, P., Pyle, R., Mitthumsiri, W., Ruffolo, D., et al. (2018). Distinct pattern of solar modulation of galactic cosmic rays above a high geomagnetic cutoff rigidity. *The Astrophysical Journal*, *858*(1), 43. https://doi.org/10.3847/1538-4357/aabd3c

Mishev, A. L., Koldobskiy, S. A., Kovaltsov, G. A., Gil, A., & Usoskin, I. G. (2020). Updated neutron-monitor yield function: Bridging between in situ and ground-based cosmic ray measurements. *Journal of Geophysical Research: Space Physics*, *125*(2), e2019JA027433. https://doi.org/10.1029/2019JA027433

Nuntiyakul, W., Evenson, P., Ruffolo, D., Sáiz, A., Bieber, J. W., Clem, J., et al. (2014). Latitude survey investigation of galactic cosmic ray solar modulation during 1994–2007. *The Astrophysical Journal*, *795*(1), 11. https://doi.org/10.1088/0004-637X/795/1/11

Owens, M. J., Barnard, L. A., Muscheler, R., Herbst, K., Lockwood, M., Usoskin, I., & Asvestari, E. (2024). A geomagnetic estimate of heliospheric modulation potential over the last 175 years. *Solar Physics*, *299*(6), 84. https://doi.org/10.1007/s11207-024-02316-9

Parker, E. (1965). The passage of energetic charged particles through interplanetary space. *Planetary and Space Science*, *13*(1), 9–49. https://doi.org/10.1016/0032-0633(65)90131-5

Picozza, P., Marcelli, L., Adriani, O., Barbarino, G. C., Bazilevskaya, G. A., Bellotti, R., et al. (2013). Cosmic ray study with the pamela experiment. *Journal of Physics: Conference Series*, *409*(1), 012003. https://doi.org/10.1088/1742-6596/409/1/012003

Potgieter, M. (2013). Solar modulation of cosmic rays. *Living Reviews in Solar Physics*, *10*, 3. https://doi.org/10.12942/lrsp-2013-3

Usoskin, I. G., Gil, A., Kovaltsov, G. A., Mishev, A. L., & Mikhailov, V. V. (2017). Heliospheric modulation of cosmic rays during the neutron monitor era: Calibration using pamela data for 2006–2010. *Journal of Geophysical Research: Space Physics*, *122*(4), 3875–3887. https://doi.org/10.1002/2016JA023819

Usoskin, I., Alanko-Huotari, K., Kovaltsov, G. A., & Mursula, K. (2005). Heliospheric modulation of cosmic rays: Monthly reconstruction for 1951–2004. *Journal of Geophysical Research: Space Physics*, *110*(A12), A12108. https://doi.org/10.1029/2005JA011250

Usoskin, I., Bazilevskaya, G. A., & Kovaltsov, G. A. (2011). Solar modulation parameter for cosmic rays since 1936 reconstructed from ground-based neutron monitors and ionization chambers. *Journal of Geophysical Research: Space Physics*, *116*(A2). https://doi.org/10.1029/2010JA016105

Usoskin, I., Koldobskiy, S., Kovaltsov, G. A., Gil, A., Usoskina, I., Willamo, T., & Ibragimov, A. (2020). Revised GLE database: Fluences of solar energetic particles as measured by the neutron-monitor network since 1956. *Astronomy & Astrophysics*, *640*, A17. https://doi.org/10.1051/0004-6361/202038272

Usoskin, I. G., Kovaltsov, G. A., Adriani, O., Barbarino, G. C., Bazilevskaya, G. A., Bellotti, R., et al. (2015). Force-field parameterization of the galactic cosmic ray spectrum: Validation for Forbush decreases. *Advances in Space Research*, *55*(12), 2940–2945. https://doi.org/10.1016/j.asr.2015.03.009

Usoskin, I. G., Solanki, S. K., Krivova, N., Hofer, B., Kovaltsov, G. A., Wacker, L., et al. (2021). Solar cyclic activity over the last millennium reconstructed from annual ^{14}C data. *Astronomy & Astrophysics*, *649*, A141. https://doi.org/10.1051/0004-6361/202140711

Väisänen, P. (2024). Synthetic 1-100 gv daily cosmic ray proton data set for 2011-2019 and 1964-2021 [Dataset]. *University of Oulu, Sodankylä Geophysical Observatory*. https://doi.org/10.23729/f2901c5a-235a-4302-b5bf-988d465d7406

Väisänen, P., Usoskin, I., Kähkönen, R., Koldobskiy, S., & Mursula, K. (2023). Revised reconstruction of the heliospheric modulation potential for 1964–2022. *Journal of Geophysical Research: Space Physics*, *128*(4), e2023JA031352. https://doi.org/10.1029/2023JA031352

Vos, E. E., & Potgieter, M. S. (2015). New modeling of galactic proton modulation during the minimum of solar cycle 23/24. *The Astrophysical Journal*, *815*(2), 119. https://doi.org/10.1088/0004-637X/815/2/119